# Colorimetric Sensor Array for Monitoring CO and Ethylene

Zheng Li[ID] and Kenneth S. Suslick*[ID]

Department of Chemistry, University of Illinois at Urbana—Champaign, 600 South Mathews Avenue, Urbana, Illinois 61801, United States

S *Supporting Information*

ABSTRACT: Developing miniaturized and inexpensive detectors remains an important and practical goal for field-deployable monitoring of toxic gases and other bioactive volatiles. CO (a common toxic pollutant) and ethylene (the phytohormone primarily responsible for fruit ripening) share the capability of strong back-π-bonding to low-oxidation-state metal ions, which has proved important in the development of metal-ion-based sensors for these gases. We report herein cumulative colorimetric sensor arrays based on Pd(II)-silica porous microsphere sensors and their application as an optoelectronic nose for rapid colorimetric quantification of airborne CO and ethylene. Quantitative analysis of two gases was obtained in the range of 0.5 to 50 ppm with detection limits at the sub-parts-per-million level (~0.4 ppm) after 2 min of exposure and ~0.2 ppm after 20 min (i.e., <0.5% of the permissible exposure limit for CO and <10% of the ethylene concentration needed for fruit ripening). We further validate that common potential interfering agents (e.g., changes in humidity or other similar air pollutants such as NO_x, SO_2, H_2S, or acetylene) are not misidentified with CO or ethylene. Finally, the sensor is successfully used for the quantification of ethylene emitted from ripening bananas, demonstrating its potential applications in the monitoring of fruit ripening during storage.
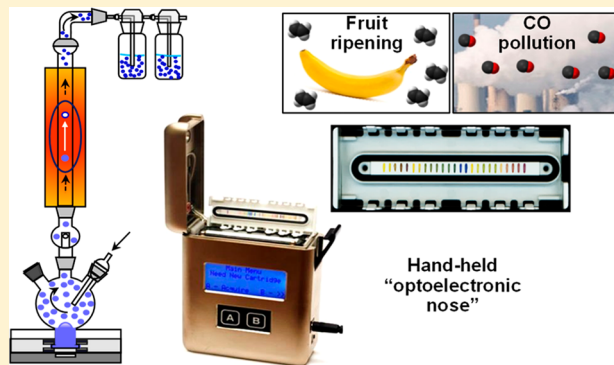
Carbon monoxide (CO) is an important cell-signaling molecule that affects various biological processes[1,2] and is also well-known as an odorless, poisonous pollutant through ligation to the iron−porphyrin complex of heme proteins. CO from incomplete combustion is responsible for ~25 000 poisonings and ~500 deaths per year in the US alone.[3,4] Although acute CO toxicity requires minutes of exposure at high concentrations (e.g., ~1000 ppm), long-term exposure to CO even at modest levels (20−50 ppm, well below the 50 ppm of the OSHA permissible exposure limit[5]) can result in toxic symptoms, including dizziness, headaches, nausea, or confusion.[6] Early detection of indoor CO at low levels is therefore of great importance for avoiding chronic household or workplace poisoning.

Ethylene (C_2H_4), on the other hand, is not particularly toxic to animals or humans (the permissible exposure level is >200 ppm), but it is the primary phytohormone used in agricultural production for ripening, and it is closely associated with nearly every development stage of plant growth, from germination to blossoming, fruit ripening, and seeding.[7] Excess concentrations of excess ethylene have a negative impact through premature spoilage of various plant products. The plant ethylene receptor is a Cu(I) protein.[7,8] Ethylene is bioactive even at low-parts-per-million levels, and it is responsible for ripening in a variety of fruits (so-called climacteric fruits, such as apples, bananas, melons, and tomatoes).[9−11]

While there are numerous approaches available for measuring gaseous CO or C_2H_4,[12−14] a pressing need for rapid, portable, selective, and sensitive detection still remains. Most of the commercial CO or C_2H_4 detectors are based on semiconducting metal oxides (mostly SnO_2),[15−17] electrochemical cells,[18,19] or chemiresistive materials (e.g., organic-conjugated-polymer[20] or carbon-nanotube[21] sensors). Those sensors, however, often require high operating temperatures; suffer from relatively poor sensitivity; or are prone to interference from other common pollutants or volatiles, including humidity changes, NO_x, SO_2, H_2S, and others.[13,22,23] Very recently, some progress has been made toward the development of CO[24−26] or C_2H_4[27] sensors using optical sensing based on colorimetric or fluorometric probes.[24−27] For example, Sancenón and co-workers have reported several Ru(II) and Os(II) complexes for colorimetric detection of CO down to the sub-parts-per-million level within a few minutes.[28−31]

What ties these two analytes together is their strong back-π-bonding during ligation with the consequent stabilization of low oxidation states and facilitation of the reduction of the metal-ion center in coordination complexes. In this manuscript, we make use of this distinctive property to create a new
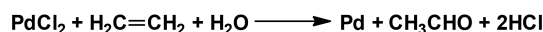
class of disposable dosimetric (i.e., cumulative) colorimetric sensor array using porous Pd(II)-silica microspheres. We have substantially improved the sensitivity and speed of response of this new class of sensors by combining pH indicators with Pd(II) complexes, and we constructed sensor arrays for CO and ethylene by facile printing of chemically responsive inks made from these microspheres.

Combined with an inexpensive hand-held optical reader, we show rapid colorimetric quantification of gaseous CO and ethylene over a broad dynamic range and even down to trace levels (500 ppb to 50 ppm). We demonstrate that this technology is a promising alternative to prior optical or electrochemical methods for the trace, quantitative analysis of CO or C_2H_4 at low-parts-per-million concentrations in terms of sensitivity, chemical specificity, accurate quantification, simplicity of array fabrication, and ease of data acquisition and analysis.

The metal ion probes have been developed for detection of CO or C_2H_4 on the basis of rationally designed metal complexes that will coordinate these analytes and whose reactivity is altered thereby, thus providing a mechanism for sensing; indeed, the first use of Pd complexes for CO detection goes back to 1947.[27,28,32−35] Inspired by this strategy, we demonstrate herein a porous-silica-based colorimetric sensor array for rapid quantitative and selective determination of CO and C_2H_4 that incorporates $PdCl_2$ combined with five pH indicators prepared by ultrasonic spray pyrolysis (Figure 1).[36−38] These sensor arrays are disposable and easily printed on surfaces of various materials, including porous polymer membranes, using standard dip-pin printing.[39,40]

The mechanism of sensing comes from the well-known reactivity of Pd(II) induced by coordination of strong back-π ligands, which leads to reduction, producing Pd metal.[35,41,42] As shown in Scheme 1, the color changes originate from both

Figure 1. Workflow diagram showing the fabrication and use of the sensor array. Porous silica microspheres were prepared by use of ultrasonic spray pyrolysis to encapsulate $PdCl_2$ and one of five pH indicators (CR, chlorophenol red; BP, bromocresol purple; BB, bromophenol blue; BXB, bromoxylenol blue; AL, alizarin) with four different concentrations of base. The arrays were printed on a polypropylene membrane, and the color changes were measured using a portable reader with a color contact image scanner. Photos of the array before and after 2 min of exposure to CO at 10 ppm are shown.

Scheme 1. Reduction of Pd(II) Involving CO or C_2H_4^{a}

$$PdCl_2 + CO + H_2O \longrightarrow Pd + CO_2 + 2HCl$$

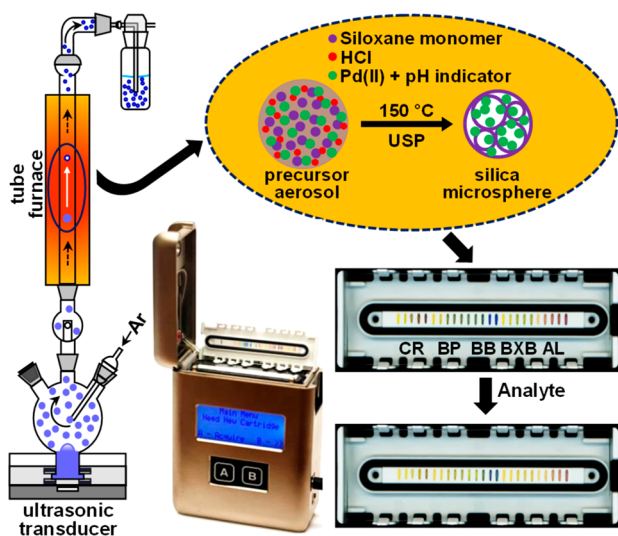$$PdCl_2 + H_2C{=}CH_2 + H_2O \longrightarrow Pd + CH_3CHO + 2HCl$$

^{a}These reactions are intermediates in standard water−gas-shift and Wacker reaction mechanisms.[35,41,42].

the reduction of the Pd(II) complex (with a characteristic color change from orange to brown) *and* the consequent increase in local acidity due to the release of HCl, thus triggering significant color changes of the pH indicator molecules throughout the silica microsphere.
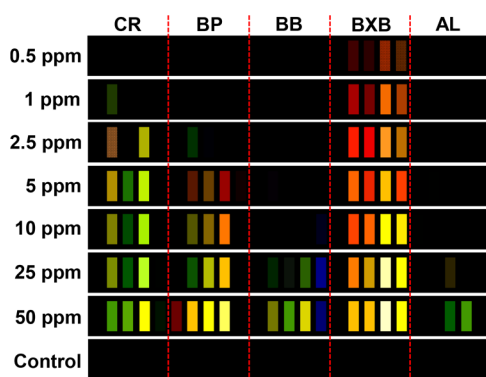
The development of colorimetric sensor arrays makes use of the wide chemical diversity available in chemically responsive dyes.[43,44] Our colorimetric sensor arrays probe a broad range of chemical interactions using a set of chemoresponsive dyes immobilized in hydrophobic matrices.[45−48] The change in colors (RGB) of the array before and after exposure to a given odorant are digitally imaged and provide a "fingerprint" that identifies the odorant by comparison to a collected library database. Colorimetric sensor arrays have proved extremely effective for identification and quantification of analytes in both gaseous and aqueous phases and have found successful application in security screening,[48−50] environmental monitoring,[51] and medical diagnosis[52] and in quality inspection of foods and drinks.[53] These sensor arrays, however, have not previously been designed to detect carbon monoxide or ethylene, either as single analytes or as parts of mixtures.

To make the sensor elements more chemically responsive to CO and C_2H_4, we have combined the colorimetric changes associated with the precipitation of Pd(0) with the use of pH-sensitive dyes to also detect the HCl produced in the reduction (Scheme 1). As such, we immobilized water-soluble Pd(II) salts (i.e., Na_2PdCl_4) together with dye molecules in porous silica microspheres (surface area ∼300 m²/g, Figure 1), following a general method of ultrasonic spray pyrolysis,[38,47] described in the Experimental Section below. Prior to printing the 25-element sensor arrays, each silica-dye solution was modified with tetrabutylammonium hydroxide (TBAH) at different molar ratios (0:1, 1:1, 2:1, 3:1, and 4:1 between TBAH and the dye entrapped in the silica microsphere), which showed varying color changes upon exposures to analytes (Figure 1).

We measured responses of the 25-element colorimetric sensor array during exposure to a wide range of CO or C_2H_4 concentrations using the recently developed portable hand-held scanner;[44,54] all gas-phase concentrations were confirmed by in-line analysis (MKS 2030 multigas analyzer). Sensor-array responses provide readily distinguishable patterns for all concentrations of CO (Figure 2) and C_2H_4 (SI Figure S1), even down to sub-parts-per-million levels. The distinctive color-difference pattern of each analyte allows for semi-quantitative detection of both CO and C_2H_4 at concentrations as low as 0.5 ppm. As shown in Figure S2, the sensor response of five silica-dye composites with different additions of TBAH proved to be optimal when the stoichiometric ratio n(TBAH)/n(dye) was 3 for all indicators except alizarin (for which the optimal ratio was 2). This is due to the structures of the different pH indicators. For triarylmethane dyes (i.e., chlorophenol red, CR; bromocresol purple, BP; bromophenol blue, BB; and bromoxylenol blue, BXB), each dye molecule contains one lactone and two phenolic groups, and the most

Figure 2. Color-difference profiles of the 25-element sensor array after 2 min of CO exposure in the concentration range of 0.5−50 ppm with an air control. Each analyte was replicated in quintuplicate. Color changes were clearly shown at or above 0.5 ppm. Those color patterns were scaled from 3 bit (i.e., 3−10) to 8 bit (i.e., 0−255) per RGB channel for display purposes; analysis used only the raw data.

responsive form is the completely deprotonated species, which requires three OH^- equivalents; in contrast, alizarin (AL) has only two phenolic groups and therefore requires less base.

We defined the overall sensor response as the Euclidean distance of the color changes of all sensor elements (i.e., square roots of the sums of the squares of all ΔRGB values). We were therefore able to quantify the color difference created by exposure to analytes: on the basis of both the 2 and 20 min response curves (Figures S3 and S4), the overall sensor responses changed monotonically with increasing concentrations of CO or C_2H_4 from 0.5 to 50 ppm; at low concentrations (below ∼2 ppm), the correlation was essentially linear.

The irreversible reactions that occur between Pd(II) and CO or C_2H_4 make the colorimetric response cumulative, which has the advantage of providing substantial improvements in the dosimetric sensitivities. For a typical cumulative sensor, the array response is generally linear as a function of dose until saturation (i.e., when all dye molecules have reacted). As shown in Figure S5a,b, our sensor array gives an essentially linear response for nearly all concentrations over 20 min of exposure, with the exception of the saturating curve found at the highest CO concentration (50 ppm). This reduction is essentially irreversible, so these sensor arrays are not meant to be reused; because the colorimetric sensor is easy to manufacture and low in cost (<20 cents for each), disposable sensor arrays are generally acceptable.[54] The array response to exposure to CO or C_2H_4 is indeed mostly irreversible (Figure S5), although upon flushing with air or nitrogen, there is a very slow reversal, probably due to loss of the HCl produced during the reduction (Scheme 1).

We estimated the limits of detection (LODs) of both analytes through quadratic fitting of all RGB channels and extrapolation of the curve to a concentration where the signal to nose ratio (S/N) is equal to 3. As a dosimetric (i.e., cumulative) sensor array (Figure S5c), detection limits can be substantially improved by increasing exposure time. LODs were calculated to be 0.35 and 0.42 ppm for CO and C_2H_4 for 2 min exposures. When the exposure time was extended to 20 min, the LODs were reduced to 0.15 and 0.17 ppm, respectively.

To assess the selectivity of the array toward CO and C_2H_4, the sensor array was tested against changes in relative humidity

(RH), and by exposure to several common air pollutants as potential interfering agents. Changes in RH are a primary disturbing factor in the performance of chemical sensors, especially among metal oxide semiconductors and conductive polymers.[13,22,23] We demonstrated through experiments that the response of our sensor array is indeed independent of changes in humidity: over a wide range of RH (10−90%, Figure S6), the response to 10 ppm C_2H_4 remained constant within a 10% relative standard deviation. It is worth noting that H_2O is a necessary component of the reaction that produces the reduction of the Pd(II) sensors. Even at 10% RH, however, the concentration of water vapor is so much larger than that of the relevant analytes (i.e., several thousand parts per million vs <10 ppm) that changes in RH do not contribute significantly to the kinetics of Pd(II) reduction and hence have no effect on the overall sensor response.

Because of the incorporation of pH-sensitive colorants in our sensors, it would have been possible that common acidic air pollutants could induce significant color changes. Because the color changes of each sensor element in response to CO or C_2H_4 arise both from the pH indicators (from changes in local Brønsted acidity) and from the reduction of Pd(II) to Pd(0) (with a color change from orange to brown), one would expect (and we observe) that responses to CO or C_2H_4 should be differentiable from any acidic interfering agents that cannot trigger such reduction. We measured sensor responses to NO_x, SO_2, and H_2S; none of those interfering agents generated color-difference patterns, even at 10 ppm, that are similar to or nearly as intense as those of CO and C_2H_4 (Figure S7). We also examined 10 ppm concentrations of acetylene and propylene for comparison with C_2H_4 (Figure S7); their responses were stronger than those of the pollutants but easily distinguishable from those of CO and C_2H_4. This selectivity originates from the differences in the strengths of the π-back-donations in the bonds formed between Pd(II) and CO, Pd(II) and C_2H_4, and Pd(II) and other potential ligands (e.g., acetylene and propylene), which is the process that facilitates the reduction of the Pd(II) complex. The nearly zero response from NO exposure is probably due to its much diminished π-back bonding; weak changes in the color patterns elicited by NO_2, SO_2, or H_2S are due either to their inherent acidity or to secondary reactions (e.g., the formation of PdS as a black precipitate upon exposure to H_2S).

In order to quantitatively demonstrate the differentiating capability of the colorimetric sensor array, a model-free (i.e., unsupervised) multivariate analysis, hierarchical-cluster analysis (HCA using minimum variance),[44,55] was employed for the assessment of the data set. As shown in Figure 3, successful differentiation was achieved among all concentrations of CO and C_2H_4, as well as among all interfering agents (at 10 ppm), analogues (at 10 ppm), and a N_2 control; the only misclusterings were observed between the similar oxide interfering agents NO_2 and SO_2.

Another chemometric method, principal-component analysis (PCA),[44,55] was also performed to group the multidimensional data set. PCA relies on the linear recombination of all dimensions in the vector space and uses variance in the array response to evaluate the relative contribution of each independent dimension; therefore, PCA allows the array to measure the dimensionality of the database. Given the limited interactions between the silica-dye composites and the analytes (i.e., Pd(II) reduction and Brønsted acid−base reaction) and the limited range of analytes, the PCA scree plot shows that
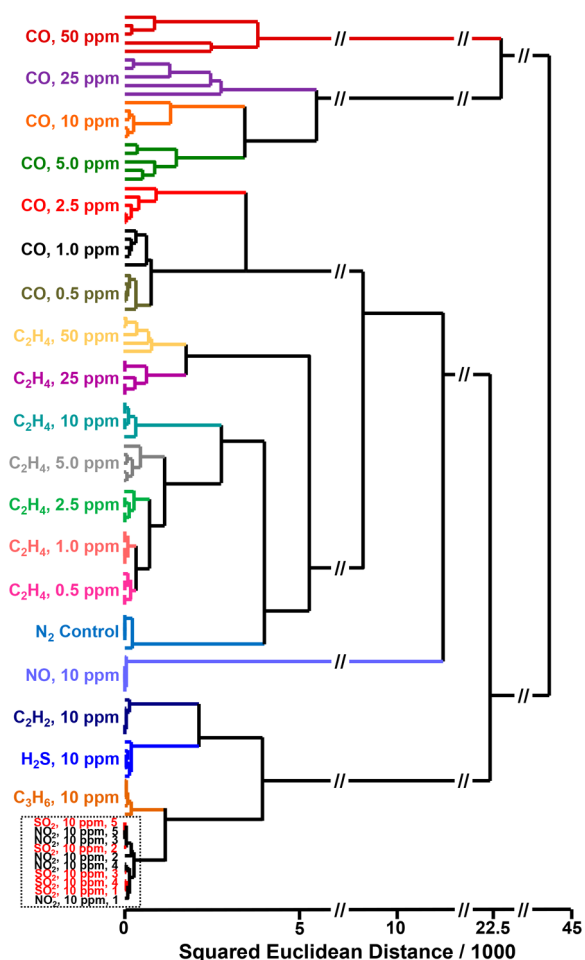
Figure 3. HCA dendrogram of quintuplicate trials of CO and C_2H_4 over the concentration range of 0.5−50 ppm, as well as of the potential interfering agents NO, NO_2, SO_2, and H_2S and analogues propylene (C_3H_6) and acetylene (C_2H_2), all at 10 ppm. No errors in clustering occur, and excellent discrimination among analytes as a function of concentration is observed, with the exception of confusion between the potential interfering agents NO_2 and SO_2.

seven principal components (PCs) are still required to account for >95% of total variance of the data (Figure S8). Compared with wider ranges of analytes (which often demand >20 dimensions), this is relatively low dimensionality.[43,44] The PCA score plot based on the first three PCs gives similar results to those from HCA: all the concentrations of CO and C_2H_4 are distinguishable from themselves and from potential interfering agents and the control after 2 min of exposure, except for a few confusions between NO_2 and SO_2.

For quantification of the predictive accuracy of the identification of analytes, we used standard support-vector-machine (SVM) analysis.[43,50,56,57] SVM analysis, a supervised method for data classification, generates an algorithm to compare an unknown analyte to an established library of known analytes; SVM is commonly used for analysis of complex multidimensional data (e.g., face and voice recognition). The results of SVM analysis are shown in SI Table S2, using a standard leave-one-out permutation model for cross-validation to test the classification of the incoming data that are not part of the training database. SVM classification is based on pairwise class prediction, and it focuses on the data most likely to be misclassified to create optimized decision boundaries that

best separate the data for each given pair of classes in high-dimensional space. The result of each pairwise comparison gives a vote to be tallied to decide the classification results. Using a standard leave-one-out permutation model, SVM analysis shows no errors out of 105 trials (i.e., the error rate is <1%, Table S2).

To test the sensor array's potential application in food and agricultural inspections, we examined the sensor array response for the determination of C_2H_4 concentrations emitted by ripening bananas. Effective monitoring of storage conditions for perishable foods is essential to the assurance of food quality and elongation of their shelf life. Ethylene is an important gaseous phytohormone that triggers the ripening process of climacteric fruits, whose ripening involves a rise in cellular respiration (e.g., apples, tomatoes, melons, and bananas), at parts per million or even sub-parts-per-million levels of C_2H_4.[58] Knowing C_2H_4 concentrations during fruit storage is therefore of real importance to the agricultural and horticultural industries. Using the sensor array, we measured C_2H_4 levels emitted both by a bunch of three bananas over 6 days of sealed storage and by a single banana over 10 days of ripening (Figures 4 and S9); for validation, results were compared to
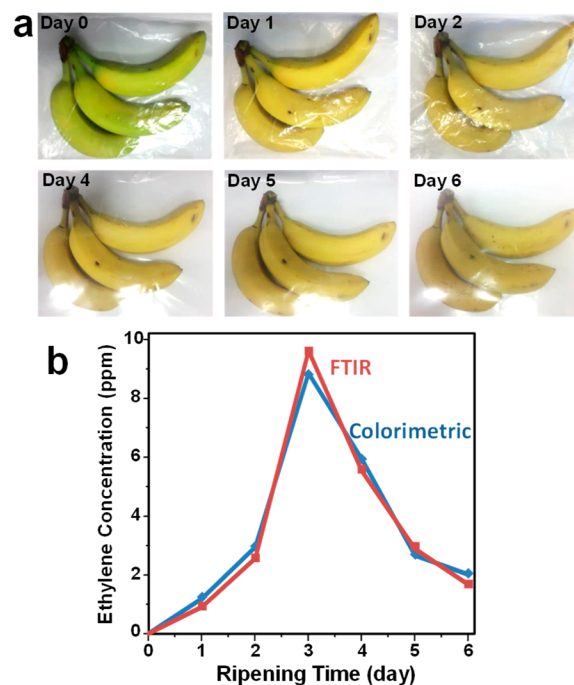
Figure 4. Monitoring of C_2H_4 concentration in the headspace above a bunch of three bananas ripening over 6 days inside a zipper-sealed polypropylene bag. (a) Photographs over 6 days. (b) C_2H_4 concentrations over the 6 days of ripening with measurements by colorimetric sensor arrays and an MKS model 2030 FT-IR multigas analyzer. Average relative standard deviations were 6 and 3.5%, respectively.

those determined by a commercial FT-IR multigas analyzer. With the bunch of three bananas ripened together in a single polyethylene zippered bag, the C_2H_4 concentration maximized on the third day (Figure 4b); for comparison, the single ripening banana under the same conditions showed a maximum C_2H_4 concentration on the eighth day (Figure S9d). Bananas undergo fast ripening when the C_2H_4 concentration grows rapidly with a color change from green to yellow; as the C_2H_4 concentration diminishes, further

ripening continues, and the color changes from yellow to dark yellow (Figures 4a and S9a). Importantly, the concentrations of C_2H_4 measured with our hand-held sensor device matched well those measured by the FT-IR multigas analyzer (Figures 4b and S9c,d).

The slower rise in C_2H_4 concentration from the single banana compared with that from the bunch and the consequently slower ripening reflects the autocatalytic ripening of climacteric fruits during storage, which is captured in such sayings as "one bad apple spoils the barrel". During the ripening process of bananas, the C_2H_4 level grows slowly at the early stage of ripening and then undergoes a rapid, short-lived increase followed by a decline (e.g., after the third day with the bunch or the eighth day with the single banana); once the climax is reached, respiration and C_2H_4-emission rates start to decrease as the fruit senesces.[11] As we see in Figures 4 and S9, the sensor array is easily responsive in the 1–10 ppm C_2H_4-concentration range needed for banana ripening.[59]

In conclusion, we have developed a simple and effective colorimetric sensor array for the rapid detection and quantitation of carbon monoxide and ethylene in the concentration range of 0.5–50 ppm. The sensor array makes use of Pd(II)-doped silica microspheres codoped with pH-sensitive dyes, which are read using a hand-held optical reader for portable measurements of the composite color changes that occur upon exposure to analytes. The array is dosimetric with limits of detection of ∼0.4 ppm for 2 min exposures to CO and C_2H_4, which are far below the permissible exposure limit of CO (50 ppm) and the required C_2H_4 concentration needed for ripening of climacteric fruits (∼10 ppm). We further tested the sensor array against potential interfering agents, including humidity, NO_x, SO_2, H_2S, propylene, and acetylene, and were able to successfully differentiate all of these analytes from CO and C_2H_4 at all concentrations, as illustrated by hierarchical-cluster analysis, principal-component analysis, and support-vector-machine analysis (with predictive accuracy >99%). Finally, through the measurement of gaseous C_2H_4 concentrations during the ripening process of bananas, we demonstrate that the inexpensive and highly portable colorimetric sensor is a promising alternative tool to other standard analytical devices (e.g., FT-IR or GC-MS) for in situ monitoring of fruit ripening or for other agricultural and horticultural applications.

■ EXPERIMENTAL SECTION

VOC-Vapor Generation, Calibration, and Sensing. All individual gas analytes at their selected concentrations were prepared by mixing their gas streams with dry and wet N_2 using MKS digital mass-flow controllers (MFCs) to reach the desired concentrations and relative humidities. Before each analysis, gas flow was equilibrated for 30 min; calibration used in-line FT-IR analysis with an MKS Multigas Analyzer (model 2030).

Preparation of Sensor Inks. The aerosol−gel synthesis of porous silica−dye microspheres followed a standard protocol using a standard ultrasonic 1.7 MHz nebulizer of the sort used in household humidifiers, as described previously.[36,37] In a typical synthesis, a precursor solution of tetraethoxysilane, ethyltriethoxysilane, ethanol, Nanopure water, and aqueous HCl was combined with $PdCl_2$, NaCl (to increase the solubility of the Pd(II)), and the five dyes. The chemical dyes and formulations used in each spot are listed in Table S1. An aerosol of the precursor solution was generated by the

nebulizer and carried in an Ar stream through a tube furnace at 150 °C at 1.0 SLPM, and the resulting microspheres were collected in a series of bubblers, centrifuged, and washed exhaustively. Printable inks were made by dispersing the microspheres in 1 mL of 9:1 (w/w) mixture of 2-methoxyethanol and polyethylene glycol (average M_w ∼ 3350) and treated with TBAH.

Sensor-Array Preparation. The linear colorimetric sensor arrays were prepared on strips of polypropylene membrane (0.2 μm pores, Sterlitech Corporation) solvent-welded to customized polycarbonate cartridges. The microsphere inks were robotically printed at 2 mm center−center distances using an array of stainless-steel bar pins (delivering ∼200 nL each) using an Array-It NanoPrint printer. The arrays were dried under vacuum for 2 h at room temperature, and stored in N_2-filled aluminized Mylar bags.

Headspace-Sampling Protocol. Bananas were placed in a sealed 10 L zippered polypropylene bag to accumulate headspace volatiles prior to the measurements. Each measurement used a fresh sensor array equilibrated to clean air for 2 min before sniffing; the array was then exposed to the banana headspace gas for another 2 min using the hand-held gas analyzer through a short Teflon tube at a flow rate of 500 sccm. Before- and after-exposure images of the array were collected using the hand-held analyzer. Five independent trials were run for each sample.

Data Analysis. Analyte response was calculated from the differences of the observed red, green, and blue values for each sensor element before and after exposure (cf. the SI for further details). HCA and PCA used MVSP software (Kovach Company). SVM analysis (Table S2) used software based on the open source LIBSVM library, using a linear kernel with default parameters.

■ ASSOCIATED CONTENT

Ⓢ Supporting Information

The Supporting Information is available free of charge on the ACS Publications website at DOI: 10.1021/acs.anal-chem.8b04321.

> Dye formulations, SVM analysis of 21 analytes; color-difference profiles of the sensor array after 2 min of ethylene exposure; optimization of response curves and chemical structures of the dyes; overall sensor response of all elements as a function of concentration; response curves of CO and ethylene in the concentration range of 0.5−50 ppm; sensor responses of 10 ppm ethylene in the presence of 10−90% relative humidity; patterns of colorimetric sensor arrays in response to different potential interfering agents; principal-component analysis (PCA) of CO, ethylene, and potential interfering agents; and monitoring of ethylene concentration in the headspace above a single banana (PDF)

■ AUTHOR INFORMATION

Corresponding Author
*E-mail: ksuslick@illinois.edu.
ORCID Ⓞ
Zheng Li: 0000-0001-9066-5791
Kenneth S. Suslick: 0000-0001-5422-0701
Notes
The authors declare no competing financial interest.

ACKNOWLEDGMENTS

REFERENCES

(1) Kim, H. P.; Ryter, S. W.; Choi, A. M. K. *Annu. Rev. Pharmacol. Toxicol.* **2006**, *46*, 411−449.

(2) Motterlini, R.; Otterbein, L. E. *Nat. Rev. Drug Discovery* **2010**, *9*, 728.

(3) Guzman, J. A. *Crit. Care Clin.* **2012**, *28*, 537−548.

(4) Carbon Monoxide Poisoning, 2017. *Centers for Disease Control and Prevention.* https://www.cdc.gov/co/surveillance/routine.htm (accessed Nov 28, 2018).

(5) Permissible Exposure Limits/OSHA Annotated Table Z-1. *OSHA.* https://www.osha.gov/dsg/annotated-pels/tablez-1.html (accessed Nov 28, 2018).

(6) Pulster, E. L.; Hillman, J. V. In *Hamilton and Hardy's Industrial Toxicology*, 6th ed.; Wiley, 2015; pp 309−316.

(7) Pech, J.-C.; Purgatto, E.; Bouzayen, M.; Latché, A. In *The Plant Hormone Ethylene*; Annual Plant Reviews; Wiley-Blackwell, 2012; Vol. 44, pp 275−304.

(8) Rodrıguez, F. I.; Esch, J. J.; Hall, A. E.; Binder, B. M.; Schaller, G. E.; Bleecker, A. B. *Science* **1999**, *283*, 996−998.

(9) Chang, C. *BMC Biol.* **2016**, *14*, 7.

(10) Sargent, S. VC-29 Ripening Tomatoes With Ethylene; Department of Horticultural Sciences, Florida Cooperative Extension Service, Institute of Food and Agricultural Sciences, University of Florida, http://ufdcimages.uflib.ufl.edu/IR/00/00/46/98/00001/CV20600.PDF, 2000; Vol. VC-29 (accessed Nov 28, 2018).

(11) Liu, X.; Shiomi, S.; Nakatsuka, A.; Kubo, Y.; Nakamura, R.; Inaba, A. *Plant Physiol.* **1999**, *121*, 1257.

(12) Fine, G. F.; Cavanagh, L. M.; Afonja, A.; Binions, R. *Sensors* **2010**, *10*, 5469−5502.

(13) Nandy, T.; Coutu, R. A., Jr.; Ababei, C. *Sensors* **2018**, *18*, 3443.

(14) Caprioli, F.; Quercia, L. *Sens. Actuators, B* **2014**, *203*, 187−196.

(15) McCue, J. T.; Ying, J. Y. *Chem. Mater.* **2007**, *19*, 1009−1015.

(16) Bhardwaj, N.; Pandey, A.; Satpati, B.; Tomar, M.; Gupta, V.; Mohapatra, S. *Phys. Chem. Chem. Phys.* **2016**, *18*, 18846−18854.

(17) Jeong, S.-Y.; Yoon, J.-W.; Kim, T.-H.; Jeong, H.-M.; Lee, C.-S.; Chan Kang, Y.; Lee, J.-H. *J. Mater. Chem. A* **2017**, *5*, 1446−1454.

(18) Lee, Y.; Kim, J. *Anal. Chem.* **2007**, *79*, 7669−7675.

(19) Zevenbergen, M. A. G.; Wouters, D.; Dam, V.-A. T.; Brongersma, S. H.; Crego-Calama, M. *Anal. Chem.* **2011**, *83*, 6300−6307.

(20) Tolentino, M. A. K. P.; Albano, D. R. B.; Sevilla, F. B. *Sens. Actuators, B* **2018**, *254*, 299−306.

(21) Esser, B.; Schnorr, J. M.; Swager, T. M. *Angew. Chem., Int. Ed.* **2012**, *51*, 5752−5756.

(22) Barsan, N.; Weimar, U. *J. Phys.: Condens. Matter* **2003**, *15*, R813−R839.

(23) Röck, F.; Barsan, N.; Weimar, U. *Chem. Rev.* **2008**, *108*, 705−725.

(24) Sun, M.; Yu, H.; Zhang, K.; Wang, S.; Hayat, T.; Alsaedi, A.; Huang, D. *ACS Sens.* **2018**, *3*, 285−289.

(25) Feng, W.; Liu, D.; Feng, S.; Feng, G. *Anal. Chem.* **2016**, *88*, 10648−10653.

(26) Lin, C.; Xian, X.; Qin, X.; Wang, D.; Tsow, F.; Forzani, E.; Tao, N. *ACS Sens.* **2018**, *3*, 327−333.

(27) Cabanillas-Galán, P.; Farmer, L.; Hagan, T.; Nieuwenhuyzen, M.; James, S. L.; Lagunas, M. C. *Inorg. Chem.* **2008**, *47*, 9035−9041.

(28) Moragues, M. E.; Esteban, J.; Ros-Lis, J. V.; Martínez-Máñez, R.; Marcos, M. D.; Martínez, M.; Soto, J.; Sancenón, F. *J. Am. Chem. Soc.* **2011**, *133*, 15762−15772.

(29) Moragues, M. E.; Toscani, A.; Sancenón, F.; Martinez-Máñez, R.; White, A. J. P.; Wilton-Ely, J. D. E. T. *J. Am. Chem. Soc.* **2014**, *136*, 11930−11933.

(30) Toscani, A.; Marín-Hernández, C.; Moragues, M. E.; Sancenón, F.; Dingwall, P.; Brown, N. J.; Martínez-Máñez, R.; White, A. J. P.; Wilton-Ely, J. D. E. T. *Chem. - Eur. J.* **2015**, *21*, 14529−14538.

(31) Marin-Hernandez, C.; Toscani, A.; Sancenon, F.; Wilton-Ely, J. D. E. T.; Martinez-Manez, R. *Chem. Commun.* **2016**, *52*, 5902−5911.

(32) Dias, H. V. R.; Wu, J. *Eur. J. Inorg. Chem.* **2008**, *2008*, 509−522.

(33) Shepherd, M. *Anal. Chem.* **1947**, *19*, 77−81.

(34) Lambert, J. L.; Wiens, R. E. *Anal. Chem.* **1974**, *46*, 929−930.

(35) Schmitt, K.; Tarantik, R. K.; Pannek, C.; Wöllenstein, J. *Chemosensors* **2018**, *6*, 14.

(36) Li, Z.; Suslick, K. S. *ACS Appl. Mater. Interfaces* **2018**, *10*, 15820−15828.

(37) Suh, W. H.; Suslick, K. S. *J. Am. Chem. Soc.* **2005**, *127*, 12007−12010.

(38) Hinman, J. J.; Suslick, K. S. *Top. Curr. Chem.* **2017**, *375*, 59−94.

(39) Li, Z.; Fang, M.; LaGasse, M. K.; Askim, J. R.; Suslick, K. S. *Angew. Chem., Int. Ed.* **2017**, *56*, 9860−9863.

(40) Lim, S. H.; Feng, L.; Kemling, J. W.; Musto, C. J.; Suslick, K. S. *Nat. Chem.* **2009**, *1*, 562−567.

(41) Horváth, I. T.; Lantos, D. In *Comprehensive Organometallic Chemistry III*; Canty, A. J., Mingos, D. M. P., Crabtree, R. H., Eds.; Elsevier: Oxford, 2007; pp 823−845.

(42) *Comprehensive Organometallic Chemistry III*; Canty, A. J., Mingos, D. M. P., Crabtree, R. H., Eds.; Elsevier: Oxford, 2007.

(43) Li, Z.; Askim, J. R.; Suslick, K. S. *Chem. Rev.* **2018**, DOI: 10.1021/acs.chemrev.8b00226.

(44) Askim, J. R.; Mahmoudi, M.; Suslick, K. S. *Chem. Soc. Rev.* **2013**, *42*, 8649−8682.

(45) Rakow, N. A.; Suslick, K. S. *Nature* **2000**, *406*, 710−713.

(46) Kemling, J. W.; Suslick, K. S. *Nanoscale* **2011**, *3*, 1971−1973.

(47) Lim, S. H.; Kemling, J. W.; Feng, L.; Suslick, K. S. *Analyst* **2009**, *134*, 2453−2457.

(48) Feng, L.; Musto, C. J.; Kemling, J. W.; Lim, S. H.; Zhong, W.; Suslick, K. S. *Anal. Chem.* **2010**, *82*, 9433−9440.

(49) Li, Z.; Jang, M.; Askim, J. R.; Suslick, K. S. *Analyst* **2015**, *140*, 5929−5935.

(50) Askim, J. R.; Li, Z.; LaGasse, M. K.; Rankin, J. M.; Suslick, K. S. *Chem. Sci.* **2016**, *7*, 199−206.

(51) Janzen, M. C.; Ponder, J. B.; Bailey, D. P.; Ingison, C. K.; Suslick, K. S. *Anal. Chem.* **2006**, *78*, 3591−3600.

(52) Li, Z.; Li, H.; LaGasse, M. K.; Suslick, K. S. *Anal. Chem.* **2016**, *88*, 5615−5620.

(53) Li, Z.; Suslick, K. S. *ACS Sens.* **2016**, *1*, 1330−1335.

(54) Askim, J. R.; Suslick, K. S. *Anal. Chem.* **2015**, *87*, 7810−7816.

(55) Stewart, S.; Ivy, M. A.; Anslyn, E. V. *Chem. Soc. Rev.* **2014**, *43*, 70−84.

(56) Ivanciuc, O. In *Reviews in Computational Chemistry*; John Wiley & Sons, Inc., 2007; pp 291−400.

(57) Li, Q.; Gu, Y.; Jia, J. *Sensors* **2017**, *17*, 272−286.

(58) Iqbal, N.; Khan, N. A.; Ferrante, A.; Trivellini, A.; Francini, A.; Khan, M. I. R. *Front. Plant Sci.* **2017**, *8*, 475.

(59) Janssen, S.; Schmitt, K.; Blanke, M.; Bauersfeld, M. L.; Wöllenstein, J.; Lang, W. *Philos. Trans. R. Soc., A* **2014**, *372*, 20130311.